

# Materials Horizons

Accepted Manuscript

This article can be cited before page numbers have been issued, to do this please use: T. Wang, H. Huang, Y. Tu, Y. Liao, C. Lai, T. Jacob, M. M. Elnagar, M. Al-Shakran and C. Hu, *Mater. Horiz.*, 2026, DOI: 10.1039/D6MH00367B.



This is an Accepted Manuscript, which has been through the Royal Society of Chemistry peer review process and has been accepted for publication.

Accepted Manuscripts are published online shortly after acceptance, before technical editing, formatting and proof reading. Using this free service, authors can make their results available to the community, in citable form, before we publish the edited article. We will replace this Accepted Manuscript with the edited and formatted Advance Article as soon as it is available.

You can find more information about Accepted Manuscripts in the [Information for Authors](#).

Please note that technical editing may introduce minor changes to the text and/or graphics, which may alter content. The journal's standard [Terms & Conditions](#) and the [Ethical guidelines](#) still apply. In no event shall the Royal Society of Chemistry be held responsible for any errors or omissions in this Accepted Manuscript or any consequences arising from the use of any information it contains.

## New Concept

View Article Online  
DOI: 10.1039/D6MH00367B

In this manuscript, we introduce hydrogen-affinity engineering, a new concept that kinetically suppresses proton-driven parasitic reactions, enabling high-voltage aqueous Zn batteries to operate stably under highly acidic conditions. By enabling stable Zn plating and stripping at pH 1.13, this approach unlocks high-voltage Zn||MnO<sub>2</sub> (~2.0 V) and Zn||PbO<sub>2</sub> (~2.35 V) batteries.

Unlike conventional strategies that focus on Zn morphology or solvation, our approach employs trace In<sup>3+</sup> ions to form a self-adaptive, low-hydrogen-affinity interphase, effectively suppressing proton-driven parasitic reactions even in highly acidic electrolytes.

Importantly, this strategy operates through two complementary mechanisms: (1) dynamic alloying during galvanostatic cycling, and (2) spontaneous replacement deposition under open-circuit conditions, enabling continuous and self-adaptive interfacial protection even during rest. This represents a paradigm shift from static protective coatings toward dynamically regenerated, proton-repelling interphases specifically designed for highly acidic environments.

By establishing hydrogen-affinity engineering as a general interfacial design principle, this work provides guidance for mitigating proton-induced parasitic reactions in Zn and potentially other proton-sensitive metals, opening new avenues for high-voltage aqueous metal batteries.



## Data Availability Statement

View Article Online  
DOI: 10.1039/D6MH00367B

The data that support the findings of this study are available in the Supporting information.



1 **Unlocking the Role of Indium Ions to Stabilize Zinc Negative Electrodes**  
2 **in Highly Acidic Electrolytes for High-Voltage Aqueous Zn Batteries**

3 Ting-Yu Wang<sup>a</sup>, Hung-Yi Huang<sup>a</sup>, Yi-Heng Tu<sup>a</sup>, Yi-Cheng Liao<sup>a</sup>, Chi-Yu Lai<sup>a</sup>, Timo  
4 Jacob<sup>b, c, d</sup>, Mohamed M. Elnagar<sup>b, c, d</sup>, Mohammad Al-Shakran<sup>b</sup>, Chi-Chang Hu<sup>a, e, f, \*</sup>

5  
6  
7 Submitted to

8 **Materials Horizons**

9 2026/02/27

10 2026/04/04 in the revised form

11 \*Corresponding Author: Chi-Chang Hu, Email: [cchu@che.nthu.edu.tw](mailto:cchu@che.nthu.edu.tw), NTHU Chair  
12 Professor

13 <sup>a</sup>Department of Chemical Engineering, National Tsing Hua University, Hsinchu 300044,  
14 Taiwan

15 <sup>b</sup>Institute of Electrochemistry, Ulm University, Albert-Einstein-Allee 47, 89081 Ulm,  
16 Germany

17 <sup>c</sup>Helmholtz-Institute-Ulm (HIU), Helmholtzstr. 11, 89081 Ulm, Germany

18 <sup>d</sup>Karlsruhe Institute of Technology (KIT), P.O. Box 3640, 76021 Karlsruhe, Germany

19 <sup>e</sup>College of Semiconductor Research, National Tsing Hua University, Hsinchu 300044,  
20 Taiwan

21 <sup>f</sup>College of Sustainability, National Tsing Hua University, Hsinchu 300044, Taiwan

22  
23 **KEYWORDS:** high voltage batteries, highly acidic, additives, In-Zn binary alloy, indium  
24 ions

25



## 1 Abstract

2 Operating Zn||MnO<sub>2</sub> and Zn||PbO<sub>2</sub> batteries in the highly acidic electrolytes enables much  
3 higher output voltages (up to ca. 2 V and 2.5 V, respectively) than the near-neutral  
4 systems, making them attractive for high-energy aqueous zinc-ion batteries. However, Zn  
5 electrodes suffer from the severe hydrogen evolution reaction (HER) and self-corrosion  
6 in acidic media, limiting the cycling stability. Here, we introduce the indium ion to  
7 stabilize the Zn electrodes in highly acidic electrolytes. During Zn plating, indium  
8 accumulates at the electrode surface to form a protective In–Zn alloy, which alleviates  
9 the HER via weakening the hydrated proton adsorption and promotes preferential growth  
10 of the Zn (002) facet, enabling highly reversible Zn plating/stripping. Moreover, the  
11 replacement deposition during rest can generate an indium-containing protection layer  
12 that mitigates the Zn self-corrosion. Consequently, Zn||Zn symmetric cells exhibit an  
13 extended cycling life approaching 3000 h (at pH 1.13), while acidic Zn||MnO<sub>2</sub> coin cells  
14 deliver a record-high discharge plateau of ~1.95 V with stable cycling over 1100 cycles.  
15 Notably, the effectiveness of In<sup>3+</sup> additives is validated in highly acidic Zn||PbO<sub>2</sub> batteries,  
16 demonstrating the general applicability. This work provides a comprehensive  
17 understanding on the In<sup>3+</sup>-regulated interfacial chemistry for high-voltage Zn batteries in  
18 highly acidic electrolyte.

19

20

21

## 22 1. Introduction

23 Developing reliable energy storage systems is crucial for enabling large-scale  
24 deployment and integration of renewable energy to achieve carbon neutrality. Among  
25 various options, aqueous zinc-ion batteries (ZIBs) have emerged as a highly promising  
26 candidate due to their safety, non-toxicity, low cost, high theoretical capacity (820 mAh  
27 g<sup>-1</sup> for the Zn negative electrode), and excellent stability under ambient conditions.<sup>1-4</sup>  
28 Among the numerous positive electrode materials for ZIBs, manganese dioxide (MnO<sub>2</sub>)  
29 stands out because of their natural abundance, environmental compatibility, and high cell



1 voltage.

2 Generally,  $\text{MnO}_2$  undergoes  $\text{Zn}^{2+}$  or proton intercalation through a one-electron  
3 transfer process in mildly acidic electrolytes, resulting in a relatively low output voltage.  
4 To increase both discharge capacity and cell voltage, highly acidic electrolytes have been  
5 introduced to activate a two-electron dissolution–deposition mechanism, enabling a  
6 remarkable theoretical specific capacity of  $616 \text{ mAh g}^{-1}$  and a high discharge voltage  
7 approaching 2 V (vs.  $\text{Zn}^{2+}/\text{Zn}$ ).<sup>5, 6</sup> Beyond the manganese-based systems, lead dioxide  
8 ( $\text{PbO}_2$ ) presents another compelling positive electrode candidate that operates  
9 exceptionally well in the relatively concentrated  $\text{H}_2\text{SO}_4$  solutions. By coupling Zn and  
10  $\text{PbO}_2$  to construct a  $\text{Zn}||\text{PbO}_2$  battery, the theoretical cell voltage can be further elevated  
11 to 2.5 V, surpassing most ZIBs.<sup>7</sup> This configuration simultaneously achieves high energy  
12 storage performance and improved environmental compatibility through substantially  
13 reducing the lead usage relative to conventional lead–acid batteries.<sup>8, 9</sup>

14 However, in highly acidic electrolytes, zinc suffers from the vigorous hydrogen  
15 evolution reaction (HER) and severe self-corrosion, which substantially shorten the  
16 cycling life and raise the safety concerns.<sup>10-12</sup> Therefore, suppressing the acid-induced  
17 corrosion and HER represents the primary challenge in stabilizing the zinc electrodes in  
18 the highly acidic environments. To address these challenges, several strategies have been  
19 proposed, including interfacial protective layers, proton barrier membranes, and battery  
20 decoupling designs.<sup>6, 13, 14</sup> Beyond them, electrolyte additives have attracted increasing  
21 attention due to their cost-effectiveness, simplicity, and high efficiency.<sup>15, 16</sup> In general,  
22 the reported mechanisms of additives fall into two categories: interfacial regulation and  
23 solvation structure optimization.<sup>17</sup> The former mean utilizes the species like ammonium  
24 acetate and cerium sulfate to adsorb on the Zn surface to guide the uniform nucleation.<sup>18-</sup>



1    <sup>20</sup> The latter strategy involves additives, particularly specific anions or polar molecules  
2    like dimethyl sulfoxide, that penetrate the Zn<sup>2+</sup> solvation shell to displace reactive water  
3    molecules, thereby minimizing the water-induced side reactions.<sup>21-24</sup> However, in the  
4    highly acidic environments, the primary challenge shifts from the merely guiding  
5    deposition uniformity to actively suppressing the vigorous HER. In such low-pH media,  
6    conventional strategies based on physical adsorption or bulk solvation regulation are  
7    often insufficient to counteract the high proton activity, because they operate indirectly  
8    and do not address the electronic origin of HER at the Zn surface.<sup>25</sup> Therefore, there is an  
9    urgent need to develop additives capable of elevating the HER overpotential at the  
10   electrode–electrolyte interface by targeting the electronic origin of HER.

11       As a result, this research introduces trace In<sup>3+</sup> as an electrolyte additive that targets  
12   the electronic origin of the HER. Compared with previously reported Zn additives and  
13   alloying strategies in the acidic electrolytes, these conventional methods still suffer from  
14   certain limitations. Many existing additive-based approaches are demonstrated in slightly  
15   strong acidic conditions (pH 2–3), and remain less explored at pH ≈ 1 required for the  
16   high-voltage Zn||PbO<sub>2</sub> batteries. This may constrain their practical applicability in the  
17   next-generation aqueous Zn systems.<sup>15, 26</sup> Conventional alloying strategies can partially  
18   address this limitation by extending the stable pH window, but their application is often  
19   restricted by the complicated fabrication processes and the potential involvement of toxic  
20   materials with environmental concerns.<sup>27, 28</sup>

21       Herein, we introduce In<sup>3+</sup> as an electrolyte additive that bridges the gap between  
22   operational simplicity and robust interfacial protection. We show that indium atoms  
23   thermodynamically accumulate at the electrode interface during Zn plating, forming a  
24   stable protective indium–zinc binary alloy surface that regulates the interfacial reactions



1 and Zn deposition. The indium–zinc binary alloy surface alleviates the HER and other  
2 parasitic reactions owing to its low affinity toward the hydrated protons ( $\text{H}_3\text{O}^+$ ), while  
3 simultaneously inducing preferential growth of the Zn (002) facet, thereby ensuring the  
4 highly reversible Zn plating/stripping. The low hydrogen affinity of indium is also evident  
5 under the open-circuit state (i.e., resting). During resting,  $\text{In}^{3+}$  undergoes the replacement  
6 deposition to form an indium-containing surface layer on the Zn electrode, may  
7 effectively protecting Zn from the self-corrosion. Benefiting from this, the Zn||Zn  
8 symmetric cell containing the  $\text{In}^{3+}$  additive exhibits an extended cycle life approaching  
9 3000 h in a highly acidic electrolyte (pH=1.13). Furthermore, the Zn|| $\text{MnO}_2$  coin cells  
10 incorporating  $\text{In}^{3+}$  deliver a high discharge plateau of nearly 1.95 V with stable cycling  
11 performance for more than 1100 cycles. In addition, the pouch-cell demonstrations  
12 validate the practical feasibility of this design with over 200 cycles. Furthermore,  $\text{In}^{3+}$   
13 was introduced as an electrolyte additive in a Zn|| $\text{PbO}_2$  battery to evaluate the universality  
14 of HER alleviation and self-corrosion inhibition under more stringent electrochemical  
15 conditions, which feature a record high discharge plateau of 2.35 V. These findings  
16 elucidate the role of  $\text{In}^{3+}$  additives as the HER and self-corrosion moderators and establish  
17 a clear mechanistic framework for their rational deployment in the high-voltage aqueous  
18 Zn-based batteries.

## 19 **Results and discussion**

### 20 **1.1 Parasitic reactions evolution**

21 Coulombic efficiency (CE) is a key indicator of the reversibility of Zn plating and  
22 stripping in aqueous electrolytes.<sup>29, 30</sup> CE loss mainly originates from the parasitic  
23 reactions such as HER and the formation of inactive (“dead”) Zn during cycling, both of  
24 which undermine long-term stability. Therefore, CE evaluation is essential and it provides



1 a reliable measure on the electrochemical reversibility of the Zn negative electrode and  
2 overall electrochemical robustness.<sup>31, 32</sup> Firstly, we prepared a highly acidic ZnSO<sub>4</sub>  
3 electrolyte containing In<sup>3+</sup> as an additive (denoted as ZSO/In<sup>3+</sup>). The optimized  
4 composition was 5 mM indium sulfate (In<sub>2</sub>(SO<sub>4</sub>)<sub>3</sub>, 1 M ZnSO<sub>4</sub>, and 0.1 M H<sub>2</sub>SO<sub>4</sub>) in  
5 aqueous solutions, according to **Figure S1** and the corresponding discussion. On the other  
6 hand, the one without indium sulfate (denoted as ZSO) was studied as a reference  
7 electrolyte.

8 CE was measured during the Zn plating/stripping process in both ZSO/In<sup>3+</sup> and ZSO  
9 electrolytes on the graphite paper at 1 mA cm<sup>-2</sup> and 1 mAh cm<sup>-2</sup>. As shown in **Figures**  
10 **1A** and **1B**, the ZSO cell short-circuited within 25 cycles, delivering an accumulated  
11 capacity of approximately 22 mAh cm<sup>-2</sup>, as indicated by the abrupt voltage drop. In stark  
12 contrast, the ZSO/In<sup>3+</sup> cell sustained more than 225 cycles with an accumulated capacity  
13 exceeding 230 mAh cm<sup>-2</sup>. The detailed galvanostatic charge–discharge (GCD) profiles  
14 measured at 1 mA cm<sup>-2</sup> further reveal that the presence of In<sup>3+</sup> significantly reduces the  
15 overpotential of Zn plating/stripping (**Figure 1C** and **Figure S2**). Specifically, the Zn/In<sup>3+</sup>  
16 cell exhibits a low overpotential of 12.2 mV, compare to the much higher value of 39.1  
17 mV at the 10<sup>th</sup> cycle observed in the ZSO electrolyte, indicating substantially improved  
18 reaction kinetics. Moreover, the CE evolution highlights a pronounced difference in  
19 stability. The ZSO cell exhibits highly fluctuating CE behavior, whereas the ZSO/In<sup>3+</sup>  
20 cell maintains a stable CE of nearly 97% throughout cycling (**Figure 1D**), highlighting  
21 the critical role of In<sup>3+</sup> in enhancing the reversibility of Zn plating/stripping. Similar  
22 trends were observed at a higher current density of 5 mA cm<sup>-2</sup>, where ZSO/In<sup>3+</sup> exhibits  
23 a higher and much stable CE, compared to ZSO, as shown in **Figure S3**.



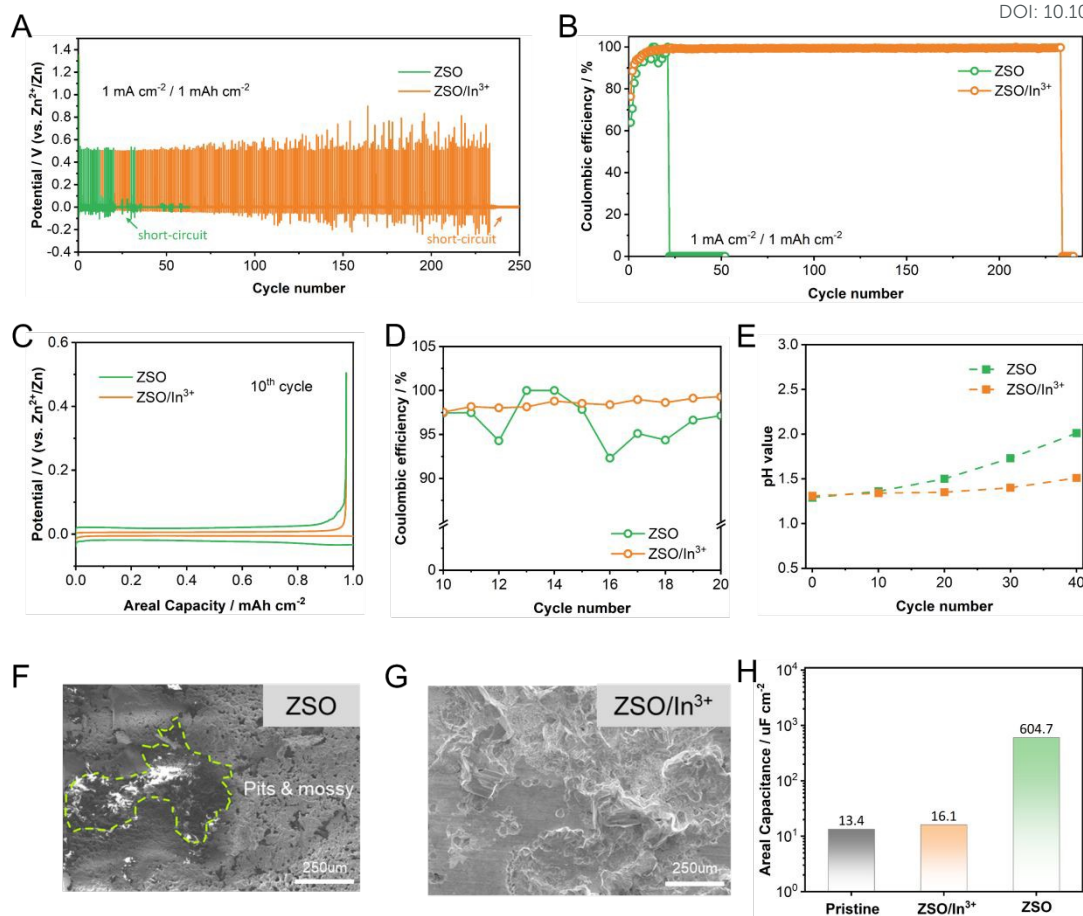
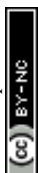
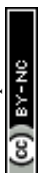


**Figure 1.** Effects of In<sup>3+</sup> additives on the Zn plating/stripping reversibility and HER alleviation. (A) The galvanostatic charge-discharge voltage profiles and (B) corresponding CE of Zn plating/stripping at 1 mA cm<sup>-2</sup> and 1 mAh cm<sup>-2</sup> in ZSO and ZSO/In<sup>3+</sup> electrolytes. (C) Detailed galvanostatic charge-discharge voltage profiles at the 10<sup>th</sup> cycle. (D) Detailed CE profiles at 1 mA cm<sup>-2</sup> and 1 mAh cm<sup>-2</sup>. (E) pH values of Zn||Zn symmetric cells during cycling. (F, G) Optical microscope images of the Zn electrode after 40 cycles in (F) ZSO and (G) ZSO/In<sup>3+</sup> electrolytes. (H) Geometric area capacitance of Zn electrodes before and after cycling in ZSO or ZSO/In<sup>3+</sup> electrolytes.

Notably, in highly acidic electrolytes, the CE loss is often attributed to the parasitic HER which consumes protons and competes with Zn deposition.<sup>15</sup> Motivated by the markedly improved CE in the presence of In<sup>3+</sup>, we therefore tracked the electrolyte pH



1 during Zn||Zn cycling as an indirect yet sensitive probe of the HER (**Figure 1E**). The  
2 ZSO/In<sup>3+</sup> electrolyte exhibits a minor pH drift, remaining at 1.51 after 40 cycles at 1 mA  
3 cm<sup>-2</sup> and 1 mAh cm<sup>-2</sup>, while an obvious increase to 2.01 is visible in the ZSO electrolyte  
4 (**Figure 1E** and the quantitative analysis of hydrogen evolution rate is provided in the  
5 **Table S1**). This observation indicates that the presence of In<sup>3+</sup> effectively alleviates the  
6 HER during cycling. The corresponding optical microscopy (OM) images corroborate  
7 this observation, showing distinct morphological differences of Zn obtained in the two  
8 electrolytes. The Zn electrode cycled in the ZSO electrolyte for 40 cycles at 1 mA cm<sup>-2</sup>  
9 and 1 mAh cm<sup>-2</sup> exhibits large surface pits and a pronounced mossy morphology (**Figure**  
10 **1F**), whereas the Zn electrode cycled in the ZSO/In<sup>3+</sup> electrolyte displays a compact and  
11 uniform surface (**Figure 1G**). To further quantify the surface evolution, the geometric  
12 area capacitance of both Zn electrodes was measured in 1 M Na<sub>2</sub>SO<sub>4</sub> to exclude the  
13 Faradaic contributions from the Zn deposition and HER in order to precisely determine  
14 the double-layer capacitance.<sup>33-35</sup> Since the double-layer capacitance is proportional to  
15 the accessible electrode surface area, changes in geometric area capacitance reflect  
16 variations in surface roughness, porosity, or morphological features during cycling.  
17 Therefore, the geometric area capacitance is considered a reliable and quantitative  
18 indicator of electrode surface area. As shown in **Figure 1H** (with detailed calculation in  
19 **Figure S4**), the geometric area capacitance of the Zn electrode cycled in the ZSO  
20 electrolyte increased by approximately 45-fold after 20 h of cycling (604.7 μF cm<sup>-2</sup>)  
21 compared to the pristine Zn electrode (13.4 μF cm<sup>-2</sup>), whereas the Zn electrode cycled in  
22 the ZSO/In<sup>3+</sup> electrolyte exhibited negligible variation (16.1 μF cm<sup>-2</sup>), indicating that the  
23 In<sup>3+</sup> additives effectively alleviate the surface roughening and stabilize the Zn surface.  
24 Importantly, the much lower geometric area capacitance reflects a much smaller  
25 electrochemically active surface area, thereby reducing the number of accessible sites for



1 proton reduction and effectively alleviates the HER and improving the overall  
2 electrochemical reversibility of the Zn electrode.<sup>36</sup>

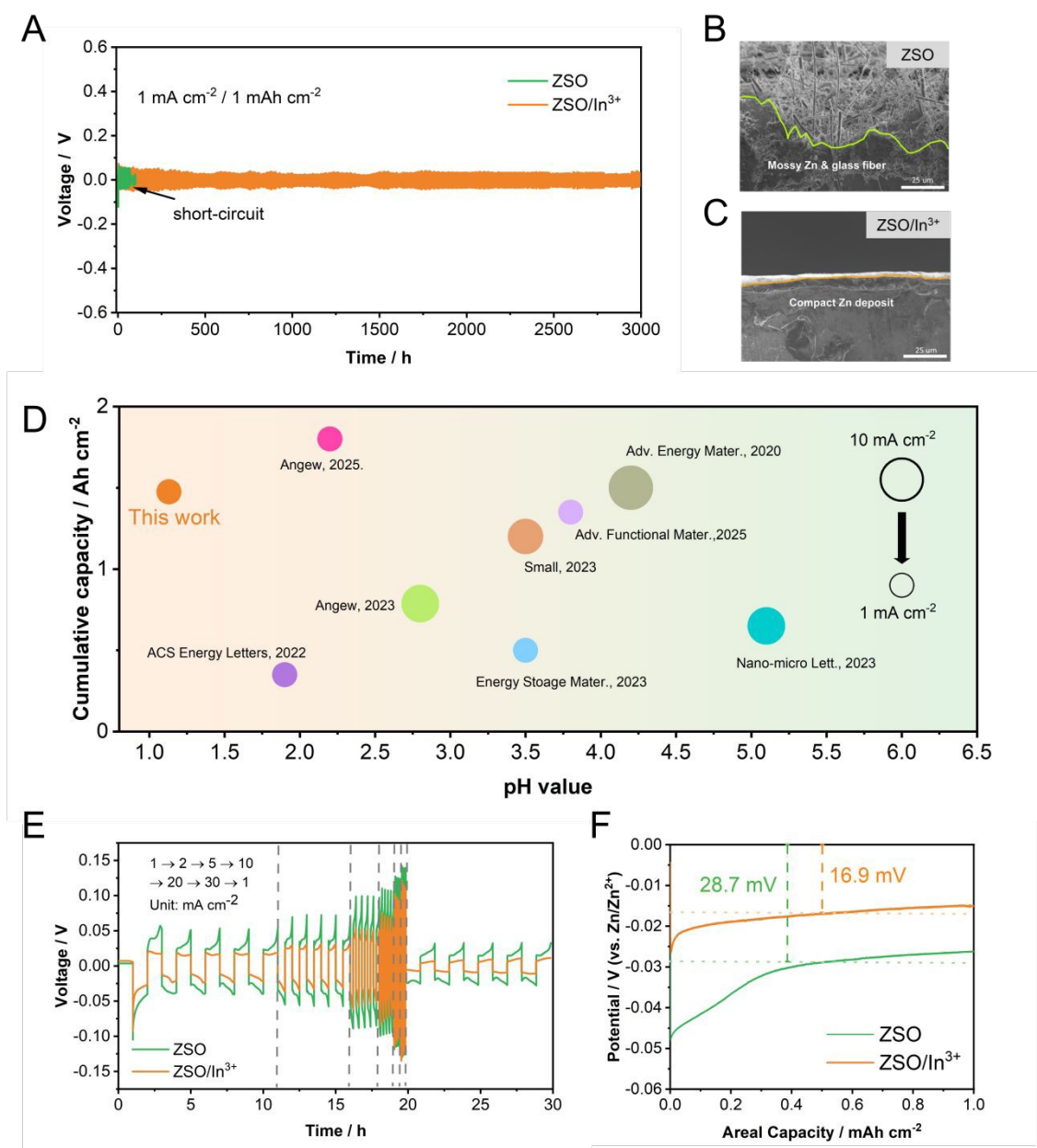
### 3 **2.2 Electrochemical Properties of Zinc electrode with Indium Additives**

4 To directly evaluate the effect of In<sup>3+</sup> additives on the intrinsic reversibility and  
5 cycling stability of the Zn electrode, symmetric Zn||Zn cells were evaluated in ZSO and  
6 ZSO/In<sup>3+</sup> at 1 mA cm<sup>-2</sup> and an areal capacity of 1 mAh cm<sup>-2</sup> (**Figure 2** and **Figure S5**).  
7 Without In<sup>3+</sup>, the ZSO symmetric cell short-circuited after about 60-h cycling, indicating  
8 rapid interfacial degradation. Strikingly, introducing In<sup>3+</sup> into the same electrolyte  
9 enabled the stable cycling for nearly 3000 h, representing an improvement of nearly 50-  
10 fold in cycle life. This dramatic enhancement originates from the In<sup>3+</sup>-regulated Zn  
11 deposition behavior. SEM images of the Zn electrodes after the 100-h cycling test in ZSO  
12 and ZSO/In<sup>3+</sup> reveal the morphology difference between two electrodes, where the one in  
13 ZSO exhibits a mossy deposit (**Figure 2B**) and the electrode in ZSO/In<sup>3+</sup> remains smooth  
14 and compact (**Figure 2C**). Such compact deposition indicates improved reversibility of  
15 Zn plating and stripping, which directly contributes to the extended cycle life.<sup>30, 37</sup> These  
16 results are in a good agreement with the previously observed high and stable coulombic  
17 efficiency obtained in ZSO/In<sup>3+</sup>, which reflects the enhanced reversibility of Zn plating  
18 and stripping. **Figure 2D** and **Table S2** compare the performance of our Zn||Zn symmetric  
19 cell using ZSO/In<sup>3+</sup> with state-of-the-art Zn||Zn symmetric cells. In summary, the system  
20 using ZSO/In<sup>3+</sup> not only operates at a relatively low pH but also maintains high  
21 cumulative capacities, setting a new benchmark for Zn symmetric cells in highly acidic  
22 electrolytes (pH < 2).

23 The rate capability and electrode kinetics of Zn in ZSO/In<sup>3+</sup> under various operating  
24 conditions were tested at current densities ranging from 1 to 30 mA cm<sup>-2</sup>. The voltage



- 1 hysteresis of the cell using ZSO/ $\text{In}^{3+}$  remains consistently lower than that of using ZSO  
 2 across the tested current densities (**Figure 2E**), indicating smaller polarization at the  
 3 electrode/electrolyte interface. This observation is consistent with the reduced  
 4 overpotential seen in **Figure 1C** and **Figure S2**, reflecting better Zn plating and stripping  
 5 kinetics in the presence of  $\text{In}^{3+}$  ions.



- 6
- 7 **Figure 2.** Long-term reversibility and rate capability of Zn symmetric cells. (A) Cycling

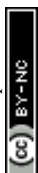


1 stability of ZSO and ZSO/In<sup>3+</sup> symmetric cells operated at 1 mA cm<sup>-2</sup> and an areal  
2 capacity of 1 mAh cm<sup>-2</sup>. (B, C) The optical microscope images of the Zn electrode after  
3 100h in (B) ZSO and (C) ZSO/In<sup>3+</sup> electrolytes. (D) Electrochemical performance of the  
4 symmetric cells compared to the state-of-the-art works in the literature.<sup>6, 38-44</sup> (E)  
5 Galvanostatic voltage profiles of these symmetric cells at various current densities (1, 2,  
6 5, 10, 20, 30, 1 mA cm<sup>-2</sup>). (F) Galvanostatic voltage profiles of a three-electrode system  
7 in ZSO and ZSO /In<sup>3+</sup> at 1 mA cm<sup>-2</sup> during the Zn plating process.

8 A three-electrode system was employed to separately evaluate the polarization  
9 behavior during the Zn stripping and plating processes. During the stripping process  
10 under anodic current, the polarization voltage in the ZSO electrolytes decreases from 32.7  
11 mV to 26.2 mV after the introduction of In<sup>3+</sup>, corresponding to a voltage reduction of 6.5  
12 mV (**Figure S6**). In contrast, during the plating process under cathodic current, the  
13 polarization voltage is reduced from 28.7 mV in ZSO to 16.9 mV in ZSO/In<sup>3+</sup> electrolytes,  
14 yielding a larger decrease of 11.8 mV (**Figure 2F**). These results indicate that indium  
15 incorporation alleviates the polarization in both Zn stripping and plating processes, while  
16 the improvement in polarization behavior is primarily associated with the Zn plating  
17 process, where the reduced cathodic polarization reflects a lower nucleation and growth  
18 barrier.

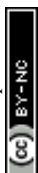
### 19 2.3 In-situ forming the In-Zn binary alloy protective layer

20 Given the pronounced stabilization of Zn electrodes enabled by In<sup>3+</sup> additives in the  
21 highly acidic electrolytes, the underlying mechanism in the electrochemical process needs  
22 to be elucidated. It is necessary to clarify whether In<sup>3+</sup> acts solely as the dissolved  
23 electrolyte additives that regulates the interfacial reactions, or it is incorporated into the  
24 Zn electrode through co-deposition for alloy formation. To address this issue, a Zn@In

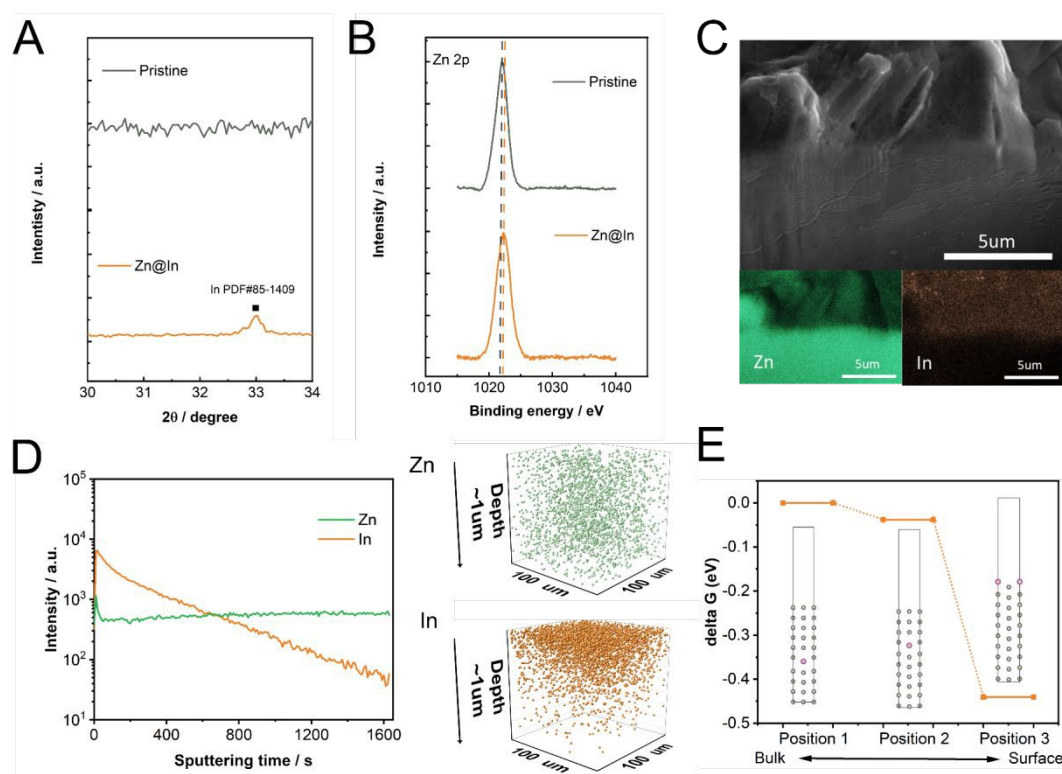


1 electrode was prepared by galvanostatic plating in the ZSO/In<sup>3+</sup> electrolyte at a current  
2 density of 1 mA cm<sup>-2</sup> with an areal capacity of 1 mAh cm<sup>-2</sup>. XRD patterns first reveal the  
3 appearance of an indium diffraction peak at ~32.9°, which is absent in pristine Zn,  
4 indicating the formation of metallic indium (**Figure 3A** and **Figure S7**).<sup>45</sup> This  
5 observation is further confirmed by XPS analysis which shows distinct In 3d signals on  
6 the Zn surface that are completely absent in pristine Zn (**Figure S8**). Meanwhile, the Zn  
7 2p peaks exhibit a positive shift of approximately 0.2 eV, moving from 1022.0 eV for  
8 pristine Zn to 1022.2 eV for Zn@In (**Figure 3B**), indicating significant interaction  
9 between Zn and In.<sup>46</sup> In addition, the surface composition quantified by XPS (**Table S3**)  
10 indicates a Zn-to-In ratio within the In-Zn solid solution region, further confirming the  
11 possible formation of the In-Zn alloy upon introduction of In<sup>3+</sup> additives (**Figure S9**).<sup>47,</sup>  
12 <sup>48</sup>

13 FIB–SEM–EDS analysis was conducted to investigate the depth-spatial distribution  
14 of indium within the deposits, revealing a pronounced surface enrichment of indium on  
15 the Zn deposits as shown in **Figure 3C**. TOF-SIMS analysis was further employed to  
16 provide a more detailed assessment of the depth-dependent distribution of indium. **Figure**  
17 **3D** demonstrates the TOF-SIMS profiles and the corresponding three-dimensional spatial  
18 distribution of indium. These results reveal a clear gradient distribution of indium, with  
19 the highest concentration near the electrolyte/electrode interface and gradually decreasing  
20 with depth over approximately 1 μm. Notably, indium signals are still detectable within  
21 the Zn deposits, indicating that indium is incorporated throughout the Zn deposition  
22 process, rather than only appearing on the surface due to replacement deposition between  
23 Zn atoms and In ions at the electrolyte/electrode interface. Collectively, these results  
24 indicate that indium participates in the electrochemical process predominantly through  
25 co-deposition with Zn, forming alloyed interfacial layer rather than remaining only in the



1 electrolyte. To elucidate the thermodynamic origin for the gradient distribution of indium,  
 2 DFT calculations were performed to evaluate the Gibbs free energy of indium atoms at  
 3 different positions within the Zn lattice (**Figure 3E**). Indium in the bulk (position 1) was  
 4 taken as the reference (0 eV), while positions closer to the surface exhibited lower Gibbs  
 5 free energies: -0.038 eV at position 2 and -0.44 eV at the surface (position 3). These  
 6 results indicate that indium atoms residing at the Zn surface exhibit the lowest Gibbs free  
 7 energy, thereby thermodynamically favoring the indium surface segregation during Zn  
 8 plating, which may contribute to alleviating the parasitic reactions.



9  
 10 **Figure 3.** Indium co-deposition and binary alloy formation on Zn electrodes. (A) XPS  
 11 spectra of Zn 2p for pristine Zn and Zn@In electrodes. (B) enlarged XRD patterns of  
 12 pristine Zn and Zn@In electrodes. (C) Cross-sectional FIB-SEM-EDS elemental  
 13 mapping of a Zn deposit prepared in the ZSO electrolyte containing 50 mM indium sulfate.  
 14 (D) The TOF-SIMS depth profiles and corresponding three-dimensional distributions of



1 Zn and In within the sputtered volume of the Zn@In electrode. (E) Gibbs free energies of  
2 indium at three positions within the Zn lattice. The purple and gray spheres represent  
3 indium and zinc atoms, respectively.

#### 4 **2.4 The hidden role of In ions**

5 To investigate whether the formation of an In-containing surface can effectively  
6 alleviate the HER on the zinc electrode, linear sweep voltammetry (LSV) was performed  
7 in 0.1 M H<sub>2</sub>SO<sub>4</sub> to evaluate the HER activity of pristine Zn and Zn@In electrodes.<sup>10, 49</sup>  
8 As shown in **Figure 4A**, the pristine Zn electrode exhibits a pronounced increase in  
9 cathodic current associated with the HER, while the Zn@In electrode shows a  
10 significantly lower current throughout the sweep. This reduced current response indicates  
11 that the In-containing surface provides the improved resistance against the HER, the main  
12 parasitic reaction on the Zn electrode. The observed HER alleviation can be understood  
13 from the perspective of metal–adsorbed H atom interactions that govern the HER activity.  
14 According to the Sabatier’s principle for effective HER metal catalysts, the binding  
15 strength between metallic catalyst atoms and adsorbed H atoms (intermediates) must be  
16 neither too strong nor too weak.<sup>50</sup> For metals such as In and Cd, weak hydrogen binding  
17 limits the Volmer step, leading to a lower HER exchange current density.<sup>51</sup> The density  
18 functional theory (DFT) further supports this HER alleviation mechanism. When indium  
19 is present on the Zn surface, the Zn@In surface exhibits a weaker binding energy toward  
20 hydrated protons (−18.1 eV) compared to pristine Zn (−25.8 eV), indicating that H<sub>3</sub>O<sup>+</sup>  
21 adsorption is energetically less favorable on Zn@In (**Figure 4B**). This reduced affinity  
22 for hydrated protons accounts for the alleviated HER activity and highlights the critical  
23 role of the In-containing surface as a HER-unfavorable protective layer in stabilizing the  
24 Zn electrode. Notably, this behavior is consistent with the Trassati’s volcano plot for the



1 HER in acidic solutions (**Figure S10**).<sup>52, 53</sup>

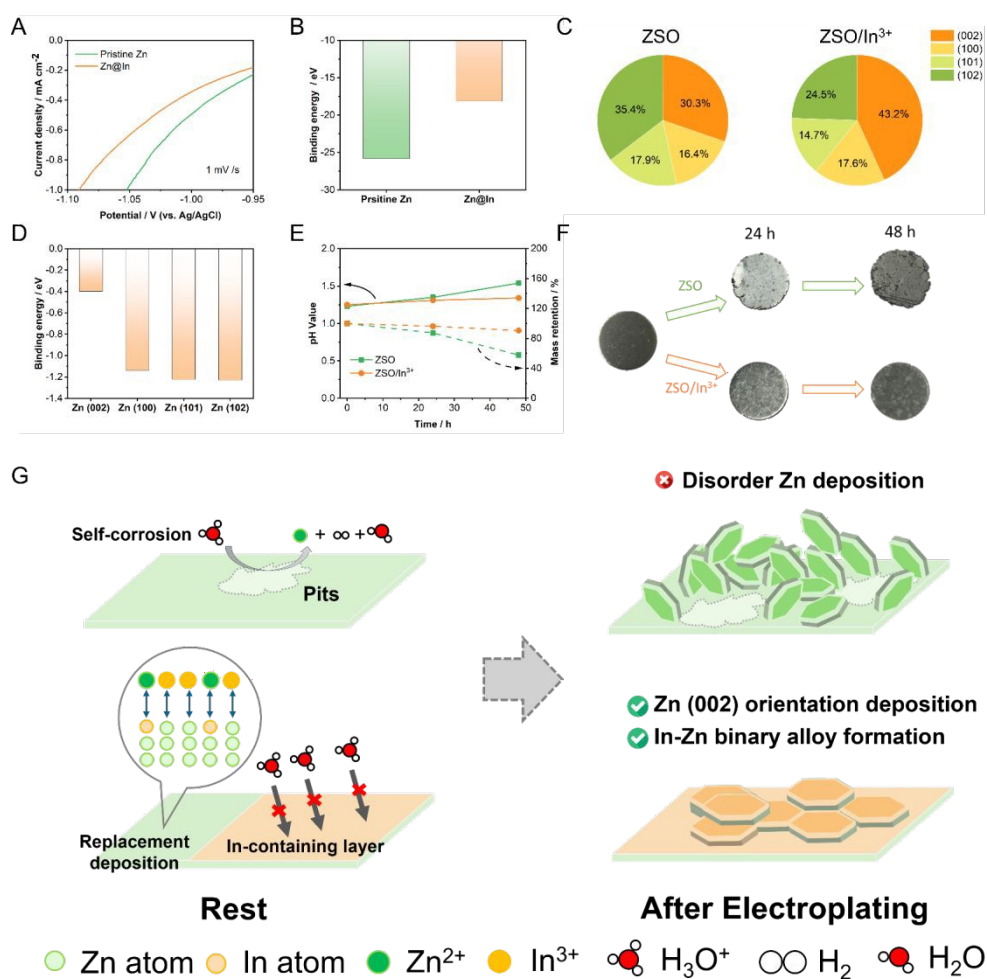
2 On the other hand, this enhanced HER alleviation arises not only from the formation  
3 of an In-containing surface but also from the preferential growth of the Zn (002) facet,  
4 which is intrinsically less active toward the HER.<sup>54, 55</sup> X-ray diffraction (XRD) analysis  
5 of Zn electrodes after cycling in ZSO and ZSO/In<sup>3+</sup> reveals such facet-selective behavior.  
6 The relative texture coefficients (RTCs) calculated from the XRD patterns show that Zn  
7 electrodes cycled in the ZSO electrolyte exhibit an RTC of 30.3% for the (002) plane after  
8 40 cycles. In contrast, the Zn electrode cycled in the ZSO/In<sup>3+</sup> electrolyte displays a  
9 markedly increased Zn (002) texture, with the corresponding RTC rising to 43.2% after  
10 cycling (**Figure 4C** and **Figure S11** for calculation details). Such facet-directed growth  
11 alleviates the HER and promotes the more reversible Zn plating/stripping.

12 The adsorption preference of indium atoms on various Zn crystal facets was also  
13 calculated through DFT (**Figure 4D**). The results reveal a pronounced facet-dependent  
14 adsorption energy, in which indium binds strongly to Zn (100), Zn (101), and Zn (102)  
15 surfaces, with binding energies of -1.14, -1.22, and -1.23 eV, respectively, whereas its  
16 interaction with the Zn (002) facet is considerably weaker (-0.40 eV). This strong facet-  
17 selective adsorption indicates that indium atoms preferentially accumulate on Zn (100),  
18 Zn (101), and Zn (102) planes, which are widely recognized to be catalytically active  
19 toward the HER.<sup>55, 56</sup> As a result, indium provides more effective passivation and  
20 protection for these HER-prone facets, thereby alleviating the parasitic HER and  
21 improving the interfacial stability of the Zn electrode.

22 In practical batteries, the Zn electrodes often experience rest periods without applied  
23 currents, during which severe self-corrosion commonly occurs due to the H<sup>+</sup> adsorption  
24 and electron transfer at the metal surface in such an acidic environment.<sup>57, 58</sup> Therefore,

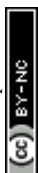


1 evaluating the corrosion resistance under the open-circuit condition is essential to ensure  
 2 the electrode stability during these rest periods. To this end, Zn foils were immersed in  
 3 ZSO and ZSO/ $\text{In}^{3+}$  electrolytes, respectively, and the variations in both pH and mass were  
 4 periodically monitored. The Zn foil immersed in the ZSO electrolyte exhibited a  
 5 pronounced decrease in mass, retaining only 57.8% of their initial mass after 48 h. On the  
 6 other hand, the one in the ZSO/ $\text{In}^{3+}$  electrolyte maintained 90.5% of its initial mass  
 7 (Figure 4E and the quantitative analysis of self-corrosion rate is provided in the Table  
 8 S4), providing the evidence consistent with corrosion alleviation in the presence of  $\text{In}^{3+}$ .  
 9 Consistent results were obtained from pH monitoring which revealed the significant  
 10 reduction in pH change in the presence of  $\text{In}^{3+}$ .



11

16



1 **Figure 4.** (A) LSV curves of pristine Zn and Zn@In electrodes measured at 1 mV s<sup>-1</sup> in  
2 0.1 M H<sub>2</sub>SO<sub>4</sub>. (B) The binding energy of H<sub>3</sub>O<sup>+</sup> on the pristine Zn and Zn@In surface. (C)  
3 The RTC values of Zn electrodes after 40 cycles in ZSO and ZSO/In<sup>3+</sup> electrolytes. (D)  
4 The binding energy of indium atoms on various Zn crystal facets. (E) The pH values and  
5 mass retention of zinc foils immersed in ZSO and ZSO/In<sup>3+</sup> electrolytes and (F) the  
6 corresponding OM images of Zn electrodes. (G) A schematic diagram of Zn resting and  
7 electroplating processes in ZSO and ZSO/In<sup>3+</sup> electrolytes.

8 The optical microscopy (OM) results further highlighted the differences in surface  
9 morphology as shown in **Figure 4F**. The Zn foil in the basic electrolyte became severe  
10 roughening after 48 h, indicative of the extensive acidic corrosion, while the Zn foil in  
11 the ZSO/In<sup>3+</sup> electrolyte maintained smooth and intact surfaces. These observations  
12 indicate that the introduction of indium ions alleviates the self-corrosion even during  
13 simple soaking without applied current. This alleviation is likely associated with the  
14 formation of indium-containing surface species which possibly mitigate the Volmer step  
15 of the HER owing to the weaker hydrogen binding affinity of indium compared with Zn  
16 metal. The formation of this indium-containing surface can be rationalized by a  
17 spontaneous replacement deposition process between Zn and In<sup>3+</sup>. This replacement  
18 deposition originates from the more positive redox potential of the In/In<sup>3+</sup> couple (-0.34V  
19 vs. SHE) compared with that of Zn/Zn<sup>2+</sup> (-0.76V vs. SHE), which thermodynamically  
20 enables the galvanic displacement of surface Zn atoms by indium species even under the  
21 open-circuit state.<sup>59</sup> The presence of indium species is further supported by the XPS  
22 analysis, which reveals the distinct In 3d signals on the Zn surface after soaking (**Figure**  
23 **S12**).

24 Overall, these results indicate that In<sup>3+</sup> stabilizes the Zn surface via multiple possible



1 mechanisms: (i) passivation of the HER-prone facets under the open-circuit state via  
2 replacement deposition to effectively alleviating Zn corrosion; and (ii) the *in situ*  
3 formation of an In-Zn binary alloy that can lower the hydrated proton activity and guides  
4 Zn (002)-oriented growth to promote the reversible Zn plating/stripping, as illustrated in  
5 **Figure 4G**.

## 6 **2.5 Full Cell Performance**

7 In order to demonstrate the practical application of indium additives in the highly  
8 acidic environment, a MnO<sub>2</sub>-free acidic Zn||MnO<sub>2</sub> battery (AZMBs) was employed, in  
9 which MnO<sub>2</sub> is *in-situ* deposited on a bare carbon substrate (MnO<sub>2</sub>-free) during the initial  
10 cycles in an electrolyte composed of 1 M ZnSO<sub>4</sub>, 1 M MnSO<sub>4</sub>, and 0.3 M H<sub>2</sub>SO<sub>4</sub> (pH =  
11 0.4) with or without 5 mM indium sulfate. The assembled AZMBs operated in both  
12 electrolytes exhibit typical galvanostatic discharge platform associated with the  
13 Mn<sup>2+</sup>/MnO<sub>2</sub> redox couple. Notably, The AZMB in the ZSO/In<sup>3+</sup> electrolyte delivers an  
14 impressive discharge plateau of ~2.0 V at 1 mA cm<sup>-2</sup> and 1.48 V at 30 mA cm<sup>-2</sup>, which is  
15 markedly higher than that in the ZSO electrolyte (1.89 V at 1 mA cm<sup>-2</sup> and 1.11 V at 30  
16 mA cm<sup>-2</sup>), as shown in **Figures 5A** and **5B**. This performance advantage is further  
17 highlighted in the comparison of plateau cell voltages across a wide range of current  
18 densities, where the ZSO/In<sup>3+</sup> cell consistently maintains a higher discharge plateau than  
19 the ZSO system (**Figure 5C**).

20 Energy efficiency (EE) is a key metric for evaluating battery performance because  
21 it represents the fraction of input energy that is effectively converted into usable electrical  
22 energy. A high EE indicates that the charging–discharging processes are extremely  
23 reversible, with minimal energy loss due to side reactions such as the HER in AZMBs.<sup>60</sup>

24 <sup>61</sup> Consistently, the AZMB operated in the ZSO/In<sup>3+</sup> electrolyte exhibits a superior energy

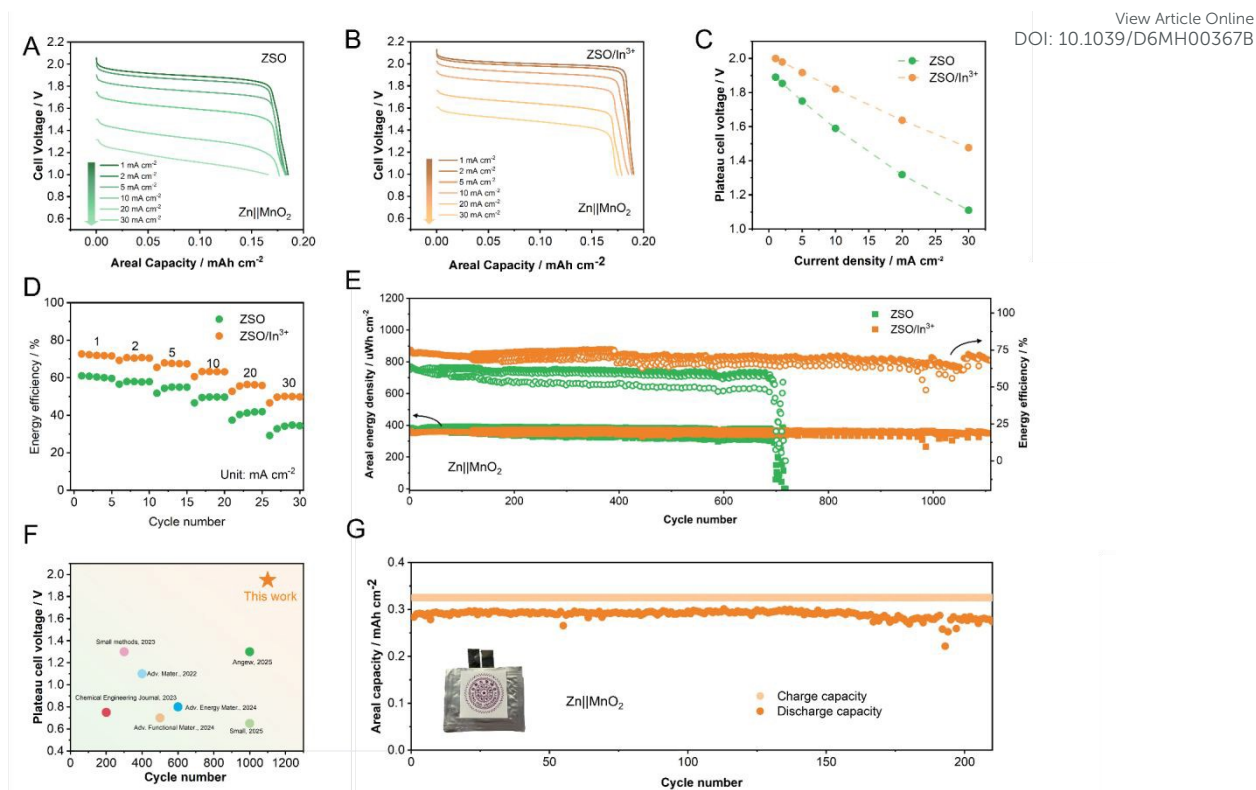


1 efficiency across all tested current densities (**Figure 5D**), reflecting the extremely high  
2 reversibility and suppressed parasitic reactions.

3 Cycling stability performance was displayed in **Figure 5E** and **Figure S13**. The  
4 cell using ZSO/In<sup>3+</sup> demonstrates excellent durability, maintaining stable cycling for over  
5 1,100 cycles at a discharge current density of 5 mA cm<sup>-2</sup> with an outstanding voltage  
6 platform of 1.95 V. In contrast, the one with ZSO shows severe voltage fluctuations and  
7 fails in fewer than 700 cycles, primarily due to the pronounced HER occurring at the Zn  
8 electrode. Notably, the achieved plateau cell voltage of 1.95 V combined with a cycle life  
9 of 1,100 cycles surpasses most previously reported aqueous ZIBs (**Figure 5F** and **Table**  
10 **S5**).

11 Pouch cells were assembled to further evaluate the practical performance of the  
12 AZMB using ZSO/In<sup>3+</sup>. Such a pouch cell sustains 200 cycles with an average discharge  
13 areal capacity of 0.325 mA h cm<sup>-2</sup>, demonstrating its promising potential for practical  
14 applications (**Figure 5G**).

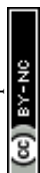




1

2 **Figure 5.** Performance of AZMBs with the ZSO and ZSO/In<sup>3+</sup> electrolytes. Galvanostatic  
 3 discharge profiles of the AZMBs with the (A) ZSO and (B) ZSO/In<sup>3+</sup> electrolytes cross  
 4 various discharge current densities. (C) Comparisons of plateau cell voltages and (D)  
 5 energy efficiency of AZMBs in ZSO and ZSO/In<sup>3+</sup> electrolytes at various current  
 6 densities.<sup>62-68</sup> (E) Cycling stability of a Zn||MnO<sub>2</sub> coin cell at 5 mA cm<sup>-2</sup>. (F)  
 7 Electrochemical performance of AZMBs with ZSO/In<sup>3+</sup> and other reported electrolyte  
 8 additives. (G) Cycling stability of acidic Zn||MnO<sub>2</sub> pouch cell at a discharge current  
 9 density of 5 mA cm<sup>-2</sup> with 0.325 mAh cm<sup>-2</sup> areal capacity.

10 This HER and self-corrosion alleviation effect of In<sup>3+</sup> additives is equally effective  
 11 under the highly acidic conditions required for PbO<sub>2</sub> conversion chemistry. The Zn||PbO<sub>2</sub>  
 12 cell was assembled in 1 M ZnSO<sub>4</sub> + 2 M H<sub>2</sub>SO<sub>4</sub> with or without 5 mM indium sulfate  
 13 (pH ≈ 0.1). The cell employing ZSO/In<sup>3+</sup> maintains over 90% EE for 50 cycles, while the  
 14 one with the ZSO electrolyte shows a lower EE and failed after only 16 cycles (**Figure**



1 **S14**). In addition, the former cell displays a stable high-voltage discharge plateau of 2.35  
2 V at the first cycle, compared to 2.22 V in the cell using the ZSO electrolyte (**Figure**  
3 **S15**).

4 Overall, the introduction of  $\text{In}^{3+}$  additives broadens the pH stability window of  
5 aqueous Zn-based batteries by alleviating the HER and self-corrosion of Zn electrode in  
6 the highly acidic media, enabling the construction of high-voltage batteries.

### 7 **Conclusion:**

8 In summary, we demonstrate that incorporating  $\text{In}^{3+}$  additives effectively stabilizes  
9 the Zn negative electrode in highly acidic electrolytes through multiple mechanisms. The  
10 formation of an indium-containing interfacial layer via replacement deposition passivates  
11 the HER-prone facets to mitigate the self-corrosion under the open-circuit state. The  
12 formation of a protective In–Zn binary alloy on the Zn surface alleviates the HER under  
13 plating. Moreover, the  $\text{In}^{3+}$  can guide the preferential growth of Zn along the (002)  
14 orientation. These integrated and synergistic mechanisms uniquely promote the Zn  
15 plating/stripping reversibility. As a result, the Zn||Zn symmetric cell exhibits an extended  
16 cycling life approaching 3000 h, meanwhile the acidic Zn|| $\text{MnO}_2$  coin cell perfectly  
17 delivers a high discharge plateau of nearly 1.95 V with stable performance over 1100  
18 cycles. Furthermore, the pouch-cell demonstration with over 200 cycles confirms the  
19 practical feasibility of this strategy. Notably, the effectiveness of  $\text{In}^{3+}$  additives is further  
20 validated in the highly acidic Zn|| $\text{PbO}_2$  conversion-type batteries, confirming the general  
21 applicability of this strategy under extreme environments. Collectively, these findings  
22 highlight the effectiveness of  $\text{In}^{3+}$  additives in enabling the highly reversible Zn  
23 plating/stripping and provide a clear framework for their application in acidic Zn|| $\text{MnO}_2$



1 and Zn||PbO<sub>2</sub> batteries with high discharge plateaus and long-term stability.

View Article Online  
DOI: 10.1039/D6MH00367B

## 2 **Author contributions**

3 Ting-Yu Wang: conceptualization, investigation, writing - review & editing, software,  
4 data curation, supervision, writing - original draft, methodology, validation, project  
5 administration, visualization, resources, formal analysis; Hung-Yi Huang:  
6 conceptualization, methodology, data curation, investigation, validation, visualization,  
7 writing - review & editing; Yi-Heng Tu: writing - review & editing, conceptualization,  
8 methodology, data curation, investigation, validation; Yi-Cheng Liao: conceptualization,  
9 methodology, writing - review & editing; Chi-Yu Lai: writing - review & editing,  
10 investigation, methodology; Timo Jacob: resources, funding acquisition, project  
11 administration; Mohamed M. Elnagar: data curation, conceptualization, methodology;  
12 Mohammad Al-Shakran: resources, formal analysis; Chi-Chang Hu: funding acquisition,  
13 writing - review & editing, methodology, supervision, resources, project administration,  
14 validation.

## 15 **Conflicts of interest**

16 There are no conflicts of interest to declare.

## 17 **Acknowledgements**

18 The financial support of this work by National Science and Technology Council (NSTC)  
19 of Taiwan under contract no. NSTC 114-2221-E-007-013 -MY3, NSTC 113-2923-E-  
20 007-007-MY3, NSTC 113-2823-8-007-003, NSTC 112-2622-E-007-032, NSTC 112-  
21 2223-E-007-006-MY3, and NSTC 112-2221-E-007-081, NSTC 112-2221-E-007-021-  
22 MY3 and Ms. Shiou-Ling Lei (instrumentation Center at NTHU) for Time-of-Flight



1 Secondary Ion Mass Spectrometer are gratefully acknowledged.

## 2 Data Availability Statement

3 The data that support the findings of this study are available in the Supporting information.

## 4 References

- 5 1. Z. Liu, M. Qin, B. Fu, M. Li, S. Liang and G. Fang, *Angewandte Chemie*,  
6 2025, **137**, e202417049.
- 7 2. Y. Song, M. Chen, Z. Zhong, Z. Liu, S. Liang and G. Fang, *Nature*  
8 *Communications*, 2025, **16**, 3142.
- 9 3. C.-Y. Lai, K.-Y. Tseng, W.-Y. Jao, T.-Y. Wang, Z.-F. He, Y.-L. Chen, H.-Y.  
10 Chen and C.-C. Hu, *Small*, 2025, **21**, e06178.
- 11 4. S. Uemura, C. Elkort, K. Than, S. Rapiere, Y. Katsuyama, J. Hui, Z. Yang,  
12 H.-Y. Huang, C.-C. Hu, M. F. El-Kady and R. B. Kaner, *Small*, **n/a**, e14911.
- 13 5. D. Chao, W. Zhou, C. Ye, Q. Zhang, Y. Chen, L. Gu, K. Davey and S.-Z.  
14 Qiao, *Angewandte Chemie International Edition*, 2019, **58**, 7823–7828.
- 15 6. H. Yang, L. Li, D. Chen, J. Wang, Y. Tan, Z. Jiang, Y. Zhang, C. Miao, W.  
16 Zhang and W. Han, *Angewandte Chemie*, 2025, **137**, e202419394.
- 17 7. Y. Xu, P. Cai, K. Chen, Y. Ding, L. Chen, W. Chen and Z. Wen,  
18 *Angewandte Chemie International Edition*, 2020, **59**, 23593–23597.
- 19 8. J. Liu, Z. Bao, Y. Cui, E. J. Dufek, J. B. Goodenough, P. Khalifah, Q. Li, B.  
20 Y. Liaw, P. Liu, A. Manthiram, Y. S. Meng, V. R. Subramanian, M. F. Toney,  
21 V. V. Viswanathan, M. S. Whittingham, J. Xiao, W. Xu, J. Yang, X.-Q. Yang  
22 and J.-G. Zhang, *Nature Energy*, 2019, **4**, 180–186.
- 23 9. D. Xu, H. Zhang, J. Xie, L. Zhou, F. Yang, J. Ma, Y. Yu, G. Wang and X.  
24 Lu, *Advanced Materials*, 2024, **36**, 2408067.
- 25 10. C.-Y. Lai, Y.-S. Liao, H.-Y. Ku, W.-Y. Jao, S. Gull, H.-Y. Chen, J.-P. Chou  
26 and C.-C. Hu, *Small*, 2024, **20**, 2401713.
- 27 11. J. Chen, W. Zhao, J. Jiang, X. Zhao, S. Zheng, Z. Pan and X. Yang, *Energy*  
28 *Storage Materials*, 2023, **59**, 102767.
- 29 12. X. Yu, Z. Li, X. Wu, H. Zhang, Q. Zhao, H. Liang, H. Wang, D. Chao, F.  
30 Wang, Y. Qiao, H. Zhou and S.-G. Sun, *Joule*, 2023, **7**, 1145–1175.
- 31 13. Y.-f. Cui, Z.-b. Zhuang, Z.-l. Xie, R.-f. Cao, Q. Hao, N. Zhang, W.-q. Liu,  
32 Y.-h. Zhu and G. Huang, *ACS Nano*, 2022, **16**, 20730–20738.
- 33 14. C. Zhong, B. Liu, J. Ding, X. Liu, Y. Zhong, Y. Li, C. Sun, X. Han, Y. Deng,  
34 N. Zhao and W. Hu, *Nature Energy*, 2020, **5**, 440–449.



- 1 15. Y. Liu, Z. Liu, Z. Xiao, Z. Lao, J. Liu, X. Xiao, Q. Fu, F. Zheng and G. Zhou, *View Article Online*  
2 *Angewandte Chemie International Edition*, 2025, **64**, e202502896. DOI: 10.1039/D6MH00367B
- 3 16. Q. Nian, X. Zhang, Y. Feng, S. Liu, T. Sun, S. Zheng, X. Ren, Z. Tao, D.  
4 Zhang and J. Chen, *ACS Energy Letters*, 2021, **6**, 2174–2180.
- 5 17. J. Wan, R. Wang, Z. Liu, L. Zhang, F. Liang, T. Zhou, S. Zhang, L. Zhang,  
6 Q. Lu, C. Zhang and Z. Guo, *ACS Nano*, 2023, **17**, 1610–1621.
- 7 18. C. Lin, X. Yang, P. Xiong, H. Lin, L. He, Q. Yao, M. Wei, Q. Qian, Q. Chen  
8 and L. Zeng, *Advanced Science*, 2022, **9**, 2201433.
- 9 19. Y. Li, P. Wu, W. Zhong, C. Xie, Y. Xie, Q. Zhang, D. Sun, Y. Tang and H.  
10 Wang, *Energy & Environmental Science*, 2021, **14**, 5563–5571.
- 11 20. A. Bayaguud, X. Luo, Y. Fu and C. Zhu, *ACS Energy Letters*, 2020, **5**,  
12 3012–3020.
- 13 21. N. Wang, S. Zhai, Y. Ma, X. Tan, K. Jiang, W. Zhong, W. Zhang, N. Chen,  
14 W. Chen, S. Li, G. Han and Z. Li, *Energy Storage Materials*, 2021, **43**,  
15 585–594.
- 16 22. L. Cao, D. Li, E. Hu, J. Xu, T. Deng, L. Ma, Y. Wang, X.-Q. Yang and C.  
17 Wang, *Journal of the American Chemical Society*, 2020, **142**, 21404–  
18 21409.
- 19 23. Q. Zhang, Y. Ma, Y. Lu, X. Zhou, L. Lin, L. Li, Z. Yan, Q. Zhao, K. Zhang  
20 and J. Chen, *Angewandte Chemie International Edition*, 2021, **60**, 23357–  
21 23364.
- 22 24. W. Zhang, J. Chen, C. Guan, T. Qiu, X. Shi, R. Chen, Z. Jiang, Q. Fu, X.  
23 Wu, H. Yang, M. Liu, P. Jiang, Y. Zhong, J. Zhou and G. He, *Angewandte*  
24 *Chemie International Edition*, 2025, **64**, e202516282.
- 25 25. C. Gao, Z. Jiang, J. Chen, K. Zhang, H. Yang, R. Chen, H. Yang, Q. Fu,  
26 Z. Li, N. Xu, M. Wang, B. Hong, F. Wu, W. Zhang and Y. Lai, *Science*  
27 *Bulletin*, 2026, **71**, 1093–1102.
- 28 26. H. Yang, L. Li, D. Chen, J. Wang, Y. Tan, Z. Jiang, Y. Zhang, C. Miao, W.  
29 Zhang, W. Han and G. He, *Angewandte Chemie*, 2025, **137**, e202419394.
- 30 27. J. Sun, X. Zheng, K. Li, G. Ma, T. Dai, B. Ban, Y. Yuan, M. Wang, M.  
31 Chuai, Y. Xu, Z. Liu, T. Jiang, Z. Zhu, J. Chen, H. Hu and W. Chen, *Energy*  
32 *Storage Materials*, 2023, **54**, 570–578.
- 33 28. P. Ruan, X. Chen, L. Qin, Y. Tang, B. Lu, Z. Zeng, S. Liang and J. Zhou,  
34 *Advanced Materials*, 2023, **35**, 2300577.
- 35 29. L. Ma, M. A. Schroeder, O. Borodin, T. P. Pollard, M. S. Ding, C. Wang  
36 and K. Xu, *Nature Energy*, 2020, **5**, 743–749.
- 37 30. J. Zheng, Q. Zhao, T. Tang, J. Yin, C. D. Quilty, G. D. Renderos, X. Liu,



- 1 Y. Deng, L. Wang, D. C. Bock, C. Jaye, D. Zhang, E. S. Takeuchi, K. J. Takeuchi, A. C. Marschilok and L. A. Archer, *Science*, 2019, **366**, 645–648.
- 2
- 3 31. Z. Wu, Y. Li and J. Liu, *Small Methods*, 2024, **8**, 2300660.
- 4 32. W.-Y. Jao, A. Aggarwal, T. K. Telmasre, L. Mishra, V. R. Subramanian, C.-C. Hu and K. J. X. Zheng, *Journal of the American Chemical Society*, 2026, **148**, 756–765.
- 5
- 6
- 7 33. J. Nan, H. Liu, W. Li, F. Zhao, L. Zhu, H. Chen and W. Li, *ACS Omega*, 2022, **7**, 41013–41020.
- 8
- 9 34. C. C. L. McCrory, S. Jung, J. C. Peters and T. F. Jaramillo, *Journal of the American Chemical Society*, 2013, **135**, 16977–16987.
- 10
- 11 35. S. Trasatti and O. A. Petrii, *Pure and Applied Chemistry*, 1991, **63**, 711–734.
- 12
- 13 36. L. Ren, Z. Hu, C. Peng, L. Zhang, N. Wang, F. Wang, Y. Xia, S. Zhang, E. Hu and J. Luo, *Proceedings of the National Academy of Sciences*, 2024, **121**, e2309981121.
- 14
- 15
- 16 37. K. Qiu, G. Ma, Y. Wang, M. Liu, M. Zhang, X. Li, X. Qu, W. Yuan, X. Nie and N. Zhang, *Advanced Functional Materials*, 2024, **34**, 2313358.
- 17
- 18 38. Y. Liu, Z. Qin, X. Yang, J. Liu, X.-X. Liu and X. Sun, *ACS Energy Letters*, 2022, **7**, 1814–1819.
- 19
- 20 39. W. Zhang, Y. Dai, R. Chen, Z. Xu, J. Li, W. Zong, H. Li, Z. Li, Z. Zhang and J. Zhu, *Angewandte Chemie International Edition*, 2023, **62**, e202212695.
- 21
- 22
- 23 40. Q. Gou, H. Luo, Q. Zhang, J. Deng, R. Zhao, O. Odunmbaku, L. Wang, L. Li, Y. Zheng and J. Li, *Small*, 2023, **19**, 2207502.
- 24
- 25 41. S. Wang, Y. Ying, S. Chen, H. Wang, K. K. K. Cheung, C. Peng, H. Huang, L. Ma and J. A. Zapien, *Energy Storage Materials*, 2023, **63**, 102971.
- 26
- 27 42. Y. M. Li, W. H. Li, X. Y. Zhang, Y. Z. Tang, Z. M. Liu, J. P. Zhang and X. L. Wu, *Advanced Functional Materials*, 2025, **35**, 2420446.
- 28
- 29 43. R. Chen, W. Zhang, Q. Huang, C. Guan, W. Zong, Y. Dai, Z. Du, Z. Zhang, J. Li and F. Guo, *Nano-Micro Letters*, 2023, **15**, 81.
- 30
- 31 44. C. Huang, X. Zhao, Y. Hao, Y. Yang, Y. Qian, G. Chang, Y. Zhang, Q. Tang, A. Hu and X. Chen, *Energy & Environmental Science*, 2023, **16**, 1721–1731.
- 32
- 33
- 34 45. P. Xiao, H. Li, J. Fu, C. Zeng, Y. Zhao, T. Zhai and H. Li, *Energy & Environmental Science*, 2022, **15**, 1638–1646.
- 35
- 36 46. S. Hsieh, T. Matsumoto, M. Batzill and B. E. Koel, *Physical Review B*, 2003, **68**, 205417.
- 37



- 1 47. J. Pstruś, Z. Moser and W. Gašior, *Applied Surface Science*, 2011, **257**,  
2 3867–3871. New Article Online  
DOI: 10.1039/D1MH00367B
- 3 48. J. Dutkiewicz and W. Zakulski, *Bulletin of Alloy phase diagrams*, 1984, **5**,  
4 284–289.
- 5 49. M. Abdallah, *Corrosion science*, 2003, **45**, 2705–2716.
- 6 50. S. Hu and W.-X. Li, *Science*, 2021, **374**, 1360–1365.
- 7 51. Z. W. Seh, J. Kibsgaard, C. F. Dickens, I. Chorkendorff, J. K. Nørskov and  
8 T. F. Jaramillo, *Science*, 2017, **355**, eaad4998.
- 9 52. P. Quaino, F. Juarez, E. Santos and W. Schmickler, *Beilstein journal of  
10 nanotechnology*, 2014, **5**, 846–854.
- 11 53. S. Trasatti, *Journal of Electroanalytical Chemistry and Interfacial  
12 Electrochemistry*, 1972, **39**, 163–184.
- 13 54. M. Zhou, S. Guo, J. Li, X. Luo, Z. Liu, T. Zhang, X. Cao, M. Long, B. Lu,  
14 A. Pan, G. Fang, J. Zhou and S. Liang, *Advanced Materials*, 2021, **33**,  
15 2100187.
- 16 55. X. Liu, Y. Guo, F. Ning, Y. Liu, S. Shi, Q. Li, J. Zhang, S. Lu and J. Yi,  
17 *Nano-Micro Letters*, 2024, **16**, 111.
- 18 56. W. Du, J. Yan, C. Cao and C. C. Li, *Energy Storage Materials*, 2022, **52**,  
19 329–354.
- 20 57. Y. Yuan, Z. Li, R. Deng, S. D. Pu, M. Walker, M. Cai, F. Wu, P. G. Bruce  
21 and A. W. Robertson, *Energy & Environmental Science*, 2025, **18**, 5610–  
22 5621.
- 23 58. R. Yao, Y. Zhao, L. Wang, C. Xiao, F. Kang, C. Zhi and C. Yang, *Energy  
24 & Environmental Science*, 2024, **17**, 3112–3122.
- 25 59. S. Chang, J. F. F. Gomez, S. Katiyar, G. Morell and X. Wu, *Journal of the  
26 American Chemical Society*, 2023, **145**, 24746–24754.
- 27 60. Z. Lin, D. Li and Y. Zou, *Journal of Energy Storage*, 2023, **74**, 109386.
- 28 61. B. Shh and G. Ee, *USA, Jul*, 1999.
- 29 62. Z. Hu, F. Zhang, Y. Zhao, H. Wang, Y. Huang, F. Wu, R. Chen and L. Li,  
30 *Advanced Materials*, 2022, **34**, 2203104.
- 31 63. Y. Wang, Y. Zhang, H. Ye, M. Wei, Y. Gu, K. Hu, S. Qu, R. Wu, X. Li and  
32 J. Zhang, *Small*, 2025, **21**, e09465.
- 33 64. J. Li, Z. Guo, J. Wu, Z. Zheng, Z. Yu, F. She, L. Lai, H. Li, Y. Chen and L.  
34 Wei, *Advanced Energy Materials*, 2023, **13**, 2301743.
- 35 65. Q. Zhao, W. Liu, X. Ni, H. Yu, C. Zhang, B. Wang, L. Jiang, H. He, Y. Chen  
36 and L. Chen, *Advanced Functional Materials*, 2024, **34**, 2404219.
- 37 66. R. Wang, J. Zhu, M. Yang and Z. Niu, *Angewandte Chemie*, 2025, **137**,



- 1 e202501327.
- 2 67. Y. Yu, P. Zhang, W. Wang and J. Liu, *Small Methods*, 2023, **7**, 2300546.
- 3 68. S. Zheng, Y. Wang, B. Luo, L. Sun, G. Duan, J. Huang and Z. Ye,
- 4 *Chemical Engineering Journal*, 2023, **473**, 145313.
- 5

View Article Online  
DOI: 10.1039/D6MH00367B

